

Extrasolar Transiting Planet Search with Subaru Suprime-Cam

Seitaro URAKAWA¹, Toru YAMADA², Yasushi SUTO³, Edwin L. TURNER⁴,
Yoichi ITOH¹, Tadashi MUKAI¹, Motohide TAMURA² and Yiping WANG⁵

¹ *Graduate School of Science and Technology, Kobe University,
1-1 Rokkodai-cho, Nada-ku, Kobe, Hyogo 657-8501*

urakawa@kobe-u.ac.jp, yitoh@kobe-u.ac.jp, mukai@kobe-u.ac.jp

² *National Astronomical Observatory of Japan, 2-21-1 Osawa, Mitaka, Tokyo 181-8588*

yamada@optik.mtk.nao.ac.jp, hide@optik.mtk.nao.ac.jp

³ *Department of Physics, School of Science, The University of Tokyo, Tokyo 113-0033*

suto@utap.phys.s.u-tokyo.ac.jp

⁴ *Princeton University Observatory, Peyton Hall, Princeton, NJ 08544, USA*

elt@astro.princeton.edu

⁵ *Purple Mountain Observatory, Chinese Academy of Sciences, China*

ypwang@pmo.ac.cn

(Received ; accepted)

Abstract

We report the results of a prototype photometric search for transiting extrasolar planets using Subaru Suprime-Cam. Out of about 100,000 stars monitored around the Galactic plane ($l = 90^\circ, b = 0^\circ$), we find that 7,700 (27,000) stars show the photometric precision below 1% (3%) for 60 second exposures which is required to detect extrasolar planets by the transit method. Thus Suprime-Cam has the photometric stability and accuracy required for a transiting planet survey. During this observing run, we detected three transiting planetary candidates (i' -band magnitude around 18.5) which exhibit a single full transit-like light curve with a fractional depth of $< 5\%$. While future photometric and/or spectroscopic follow-ups remain to be done, the estimated parameters for the three systems are consistent with planetary companions around main-sequence stars. We also found two eclipsing binary candidates and eleven variable stars exhibiting W UMa-like light curves.

Key words: stars: binaries: eclipsing — stars: planetary systems — techniques: photometric

1. Introduction

Since the first discovery in 1995 (Mayor, & Queloz 1995), more than 170 extrasolar planets around main sequence stars have been reported so far. While a majority of them were discovered by the radial velocity method, the transit method, i.e., detecting a small decrement in stellar light due to occultation by planets, provides a unique complementary means to estimate the precise radius and orbital inclination of those planets which exhibit transit. Combined with the radial velocity data, the absolute mass, the semi-major axis, the orbital period, and the mean density of the transiting planets are determined. The transit method is particularly suited for detecting “very hot Jupiters” (gas giant planets with an orbital period in the range of $1 \text{ day} \leq P \leq 3 \text{ days}$) and “hot Jupiters” ($3 \text{ days} < P \leq 9 \text{ days}$) (Gaudi, Seager, & Mallén-Ornelas 2005).

The main difficulties for the transit method are two-fold; the geometrical probability of a transit is small, and the photometric accuracy required to detect the typical transit depth ($\sim 1\%$) is demanding. This implies that wide-field accurate photometric monitoring is necessary for successful detection of planets using the transiting method. This is why only six extrasolar planets have been discovered first by the transit method, and then confirmed by the subsequent follow-up by the radial velocity measurement (3 additional transiting planets were discovered first by the radial velocity method, and their photometric transit signatures were found later).

Five out of the six confirmed transiting planets were discovered by the Optical Gravitational Lensing Experiment (OGLE) team (Udalski et al. 2002a; Udalski et al. 2002b). Indeed they reported more than 130 extrasolar planet candidates from about 150,000 stars which were observed with high photometric precision of 0.015 mag or better. Follow-up observations using the radial velocity method have so far confirmed three very hot Jupiters and two hot Jupiters from the candidates (Konacki et al. 2003a; Konacki et al. 2003b; Pont et al. 2004). The single remaining transiting planet was discovered by the Trans-Atlantic Exoplanet Survey network (TrEs) using small-aperture (10cm), wide-field (6°) CCD-based systems (Alonso et al. 2004).

A number of transit search programs are currently on-going: the Extrasolar Planet Occultation Research

(EXPLORE) project (Mallén-Ornelas et al. 2003) conducts deep transit searches of the Galactic plane using the MOSAIC II camera at the CTIO 4 m telescope and the CFH12K camera at the 3.6 m Canada-France-Hawaii Telescope. Hood et al. (2005) observed NGC 6940 using the 2.5 m Isaac Newton Telescope with its Wide Field Camera, a mosaic consisting of four 2048×4096 pixels CCDs. The MOA-I project observed 14 Galactic Bulge fields using the 61 cm Boller and Chivens Telescope at the Mt. John University Observatory with three 2048×4096 pixels CCDs (Abe et al. 2005). SuperWASP (Christian et al. 2004), Vulcan (Borucki et al. 2001), and others are also conducting very wide-field transit surveys similar to TrEs. While transiting planet candidates have been reported by these programs, the existence of the planets have not been confirmed yet.

Transit search space missions are also planned, including COROT (French Space Agency CNES, with participation of Austria, Belgium, Brazil, Germany, Spain, ESP and ESTEC) and KEPLER (NASA). These missions are expected to achieve a photometric precision up to 0.1%, and aim at detecting terrestrial planets in the habitable zone of their primary stars by the photometric transit method (Bordé et al. 2003; Basri et al. 2005).

In this paper, we describe a prototype transit search using Subaru Suprime-Cam carried out in 2002. While our observing run covered only a small range in the time domain (15 observing hours in total over 4 consecutive nights), the field-of-view is significantly wider ($34' \times 27'$), and the survey magnitude is deeper than those of OGLE and EXPLORE. Thus we mainly look for single transit events, and perform a serious attempt to test the feasibility of the photometric transiting planet search using the Subaru Suprime-Cam for the first time.

The rest of the paper is organized as follows; section 2 describes our observational strategies and data reduction procedures. In section 3, we discuss the achieved photometric precision. Section 4 presents candidate transiting objects; we found three single transit objects (likely candidates for extrasolar planets) and two double transit objects (possibly eclipsing binaries). Assuming circular orbits, we estimate the radii and the orbital elements of the companions. Finally, section 5 is devoted to a summary and further discussion. We also discovered eleven W UMa-like eclipsing binary systems, which are reported in the Appendix.

2. Observations and Data Reduction

2.1. Transit Search

In order to maximize the number of available stars, we selected a region of $34' \times 27'$ at the Galactic plane centered at $l = 90^\circ$, $b = 0^\circ$ for our photometric survey. We call it the Extrasolar Planet-field (ESP-field). The field was imaged with Suprime-Cam on the 8.2m Subaru Telescope which consists of 5×2 CCD chips with 2024×4048 pixels each. Thus the detector scale corresponds to $0''.202$ per pixel. We repeated photometric observations of the field with 60 second exposures and read-out times of 60 seconds each for 6 hours on September 28 and 29, 2002, and for 1.5 hours on October 1 and 2, 2002.

The fractional transit depth ΔF is expressed as

$$\Delta F = \left(\frac{R_p}{R_*} \right)^2, \quad (1)$$

where R_p is the radius of a planet and R_* is the radius of a parent star; the depth is approximately 1 % for a Jupiter-size planet orbiting around a Sun-like star. Equation (1) indicates that relatively small-size stars, such as late-type dwarfs, are better suited for transit detection. Since late-type dwarfs are brighter at longer wavelength, we chose i' -band for the transit photometry; z' -band is expected to be seriously compromised by high sky noise, and also the density of stars in the z' -band image is too high (confusion limit). In order to avoid the effects of any systematic errors in flat fielding, we did not conduct dithering and tried to observe stars at constant position on the CCD. We obtained 383 frames in the i' band for the entire observing run. Excluding seven frames which suffered from the telescope tracking errors, we used 376 images to search for transit events. The sky was clear on September 28, October 1 and 2, but on September 29 there were occasionally thin clouds. The seeing was approximately 0.5-0.8 arcsec during the observing runs. We use GD 248 as a standard star (Oke 1990) to determine the zero point of the i' -band photometry.

Bias was estimated from the overscan region and subtracted from each frame. In carrying out this standard procedure, we used IRAF package¹ for i' -band images and the Suprime-Cam Deep Field REDuction (SDFRED) package (Yagi et al. 2002; Ouchi et al. 2004) for multicolor photometry. The dark current is completely negligible for 60 second exposures (Miyazaki et al. 2002). The median of normalized dome frames was used as the flat frame. An example of the reduced image of chip 2 for the i' band is shown in Figure 1. This image was obtained on September 29 and the field-of-view is 1/10 of the total (10 chips).

We carried out aperture photometry using the IRAF package. The number of identified point sources exceeds 100,000. We selected a value of 10 pixels for the aperture radius (i.e., approximately 3 times of FWHM for the PSF).

¹ IRAF is distributed by the National Optical Astronomy Observatories, which are operated by the Association of Universities for Research in Astronomy, Inc., in cooperation with the National Science Foundation.

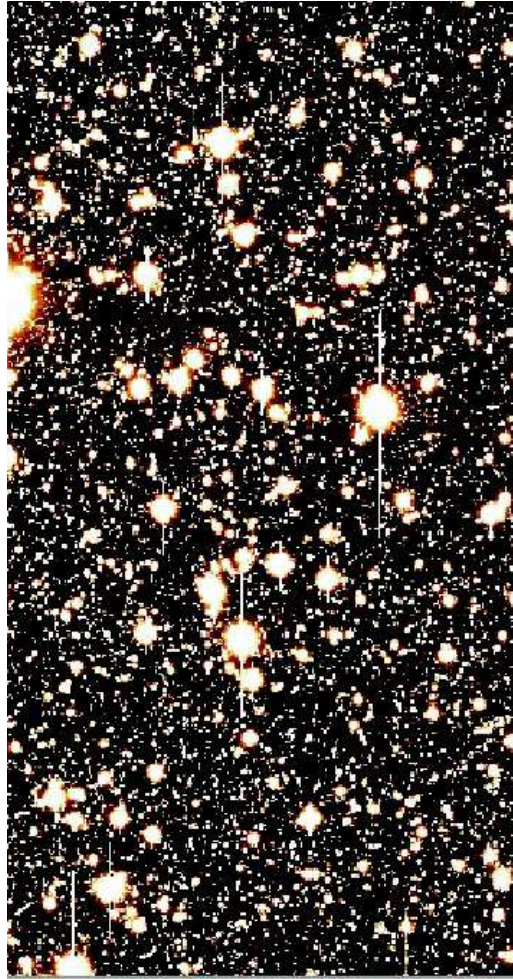


Fig. 1. An example of the reduced i' -band image for chip 2. The field of view of this image approximately $7' \times 13'$. The entire field of view of Suprime-Cam consists of ten chips (each chip has 2048×4096 pixels), and thus ten times as large as this image. The entire observed region (Esp-field) is centered at the Galactic plane of $l = 90^\circ$, $b = 0^\circ$.

Those objects with their i' -band magnitudes satisfying $18 \leq i' \leq 23$ were analyzed; we excluded $i' \leq 18$ objects because of flux saturation, and $i' \geq 23$ objects because of insufficient counts for the accurate photometry.

Change in atmospheric airmass is the primary source of absolute fluctuation in the light curves. In order to determine the atmospheric change, we select more than 200 stars per CCD chip image as references. We calculated the weighted mean fluxes of these reference stars weighted by the flux error, which are represented by Poisson noise and sky noise for each star. While short-period variable stars might be included in the reference stars, they are very rare and their contribution is expected to be negligible; the fractional ratio of W UMa-like eclipsing variables, whose periods typically range between 0.2 and 1.0 day, is approximately one in 250-300 main sequences. After correcting for the atmospheric airmass and transparency, we compute the fluxes of each star for every frame, and define the photometric precision for each star as the standard deviation among all the frames on September 28 and 29. More specifically the photometric precision is given as

$$\sigma = \sqrt{\frac{1}{n} \sum_{i=1}^n (F_i - \bar{F})^2} . \quad (2)$$

Here, σ is the photometric precision and, n is the number of frames for each night and, F_i and \bar{F} are the calibrated fluxes of each star for every frame and the mean fluxes of each star for every night, respectively.

2.2. Multicolor Photometry

We conducted multicolor photometry in the B , R_c , z' bands to determine spectral types of the stars. We obtained one image in each band. We did not observe reference stars for these bands (except for i'). Instead we used the mean

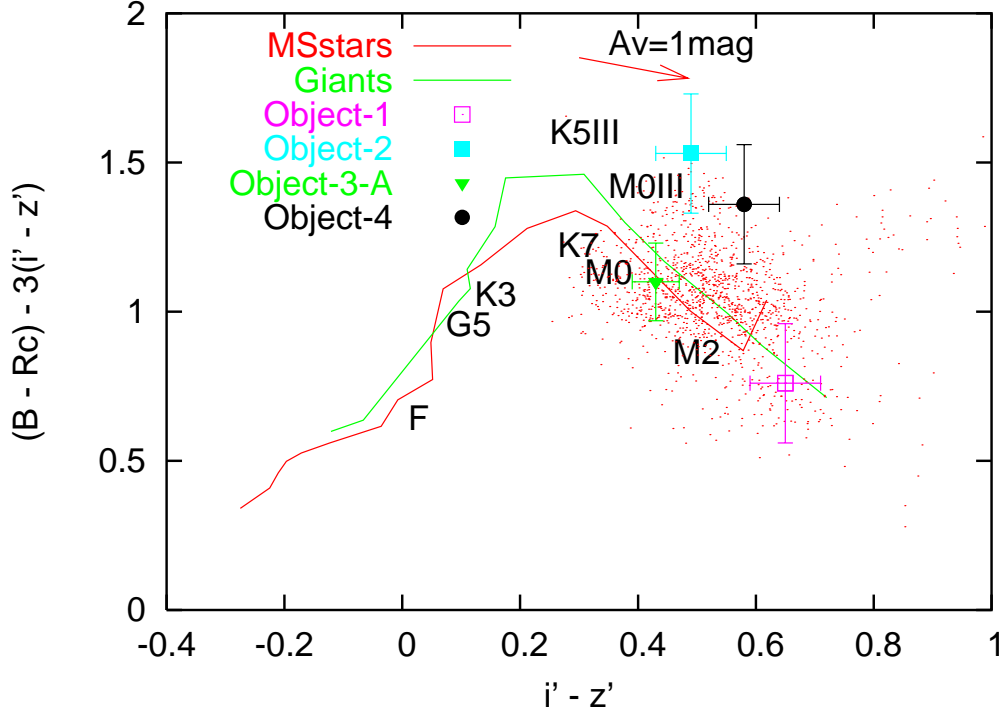


Fig. 2. Color-Color diagram for objects on chip 4 and transiting candidates discussed in §4. We plot only good photometry objects whose magnitude error is less than 0.055 magnitude and 0.2 magnitude for $i' - z'$ and $B - R_c - 3(i' - z')$, respectively. The red and green lines indicate the positions of the unreddened main sequences and giants, respectively (Bessell 1990; Fukugita et al. 1996). The arrow represents the reddening vector.

flux of reference stars in the Subaru/XMM-Newton Deep Survey Field (SXDS-field) observed on the same nights as our observing run (Sekiguchi et al. 2006, in preparation) in order to determine the zero point in the B , R_c and z' bands. From the inferred spectral type of each star, we estimate its radius and mass approximately. Moreover, we infer the distance of objects through the apparent magnitude and the typical absolute magnitude for the spectral type.

Figure 2 shows the color-color diagram for detected stars in chip 4 and our transiting candidates in §4. In the figure, the red and green lines correspond to the positions of the unreddened main sequence and giant stars, respectively. The arrow in Figure 2 is the reddening vector. We set the y-axis as $B - R_c - 3(i' - z')$ in order to clarify the locations of different spectral types just for illustrative purposes. Figure 2 indicates that most of the monitored stars are of FGKM types, but that their luminosity classes are difficult to infer from the multicolor photometry alone.

3. Photometry

3.1. Photometric Precision

Figure 3 shows the photometric precision for each star (defined in §2.1) on chip 2 as a function of its i' -band magnitude. We note that all ten CCD chips show similar photometric precisions. The green line indicates the theoretical lower bound, the Poisson noise of the stellar fluxes and the typical sky noise in the imaging data on September 28. Clearly the photometric precision of most stars is close to the theoretical limit, and a photometric precision as small as 0.4% is achieved for stars of $i' \sim 18$. Stars of $i' \leq 20$ lie significantly above a photometric precision of 10% due to the contamination of the brightness of close saturated stars.

Figure 3 also suggests that the photometric precision on September 29 is not better than that on September 28 due to the occasionally thin clouds. However, since the influence of a little bad weather on September 29 is a small, the photometric precision on September 29 is enough to detect extrasolar planets. Among more than 100,000 stars within the field of view, 27,000 objects have a photometric precision less than 3.0% for each 60 second exposure.

Table 1 shows the resulting number of stars which achieve a given photometric precision. For reference, very hot Jupiters and hot Jupiters discovered by the OGLE and TrEs exhibit a flux decrease less than 3%. Moreover, Gaudi, Seager, & Mallén-Ornelas (2005) estimated that the ratio of main sequence FGK stars which accompany transiting very hot Jupiters is approximately one in 3300-6700. Therefore the photometric precision and the number of stars in

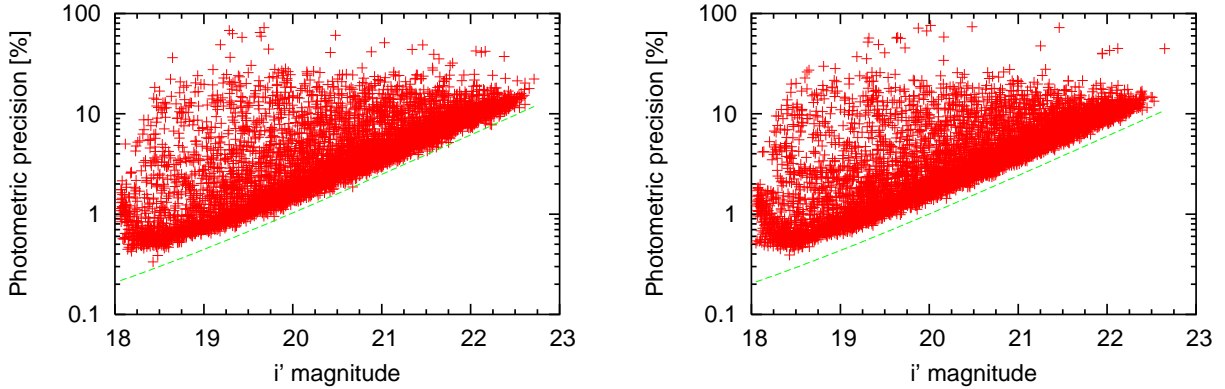


Fig. 3. Magnitude vs photometric precision for objects detected in chip 2 on September 28 (*Left*) and September 29 (*Right*).

Table 1. Summary of statistics for mean photometric precision achieved in the September 28 and 29 run.

Photometric precision	$\leq 5.0\%$	$\leq 3.0\%$	$\leq 2.0\%$	$\leq 1.5\%$	$\leq 1.0\%$	$\leq 0.50\%$
Number of stars	41,000	27,000	18,000	13,500	7,700	1,000

this prototype survey are sufficient for detecting very hot Jupiter candidates.

3.2. Selection of Candidates

Typical transit durations of the previously detected systems (Udalski et al. 2002a; Udalski et al. 2002b; Alonso et al. 2004) is a few hours. Thus we define transit candidates as light curves that have more than continuous fifteen data points (approximately continuous 30 minutes data points) which exhibit more than a 1σ flux decrement with respect to the average flux during the observing run. According to the selection criteria, we are left with around 1,000 objects out of more than 100,000 objects. We then inspected the light curves all selected objects by eye. Independently, in order to detect periodic variable stars and double transit events, we conducted period analysis using the phase dispersion minimization (PDM) algorithm described by Stellingwerf (1978). This algorithm minimizes scatter for a given data set phased to a series of test periods. The likelihood of a given test period is given by the parameter Θ . The minimum value for Θ represents the minimum dispersion of data points for a given period. We selected around 2,000 objects with Θ less than 0.5, from more than 100,000 objects, as candidates for double transit objects and variable stars. We consider objects with full double decrements in stellar light as double transit objects. However, the folded light curves for double transit objects did not cover the full phase. Next, we selected objects with sine-like light curves as W UMa eclipsing binary candidates. Although the period of those eclipsing binary candidates are estimated by the PDM method, the true period might actually be commensurate with the estimated period. For this reason, the Lomb periodogram method (Lomb 1976; Press et al. 1992) is employed for W UMa eclipsing binary candidates. The spectral power obtained by this method gives the statistically most significant period. Finally, we determine the W UMa eclipsing binary candidates according to the following criteria, (1) the fluxes were not contaminated by nearby stars, (2) the objects were detected with all bands, and (3) the data points covered approximately the full phase.

3.3. Estimation of Orbital Elements

Detections of multiple photometric transit events and extensive radial velocity follow-up are required to accurately determine orbital elements of a companion around a parent star. Approximate values, however, may be estimated even from the light curve of a single transit event, assuming that (1) the parent star is dwarf, (2) M_* and R_* (M_* is the mass of the parent star and R_* is the radius of the parent star) are inferred from the spectral type (for instance, Cox 2000), (3) the companion has a circular orbit, and (4) the mass of the companion satisfies $M_p \ll M_*$ (see, for instance, Seager & Mallén-Ornelas 2003). Then the orbital period P , the semi-major axis a , and the inclination of the orbital plane with respect to the line of sight can be explicitly written as

$$P = \frac{M_* G \pi (t_T^2 - t_F^2)^{\frac{3}{2}}}{R_*^3 32 (\Delta F)^{\frac{3}{4}}}, \quad (3)$$

$$a = \left(\frac{P^2 G M_*}{4\pi^2} \right)^{\frac{1}{3}}, \quad (4)$$

Table 2. Orbital elements for extrasolar planets and their estimated orbital elements using equations (1) and (3) to (5).

Object	P		a		i		ΔF	t_T	t_F
	(observed estimated)		(observed estimated)		(observed estimated)				
	[day]		[AU]		[°]		[%]	[min]	[min]
OGLE-TR-10b ^a	3.101386	2.3	0.04162	0.034	89.2	86	1.61	174	141
OGLE-TR-56b ^b	1.2119189	1.3	0.0225	0.024	81	81	1.32	113	71
OGLE-TR-111b ^c	4.01610	3.8	0.047	0.044	86.5-90	88	1.46	164	124
OGLE-TR-113b ^d	1.43250	1.5	0.0228	0.023	85-90	87	2.10	114	82
OGLE-TR-132b ^d	1.68965	2.4	0.0306	0.039	78-90	84	0.70	165	125
TrES-1 ^e	3.030065	3.1	0.0393	0.039	88.5	89	1.69	154	116

^a Konacki et al. 2005, ^b Torres et al. 2004, ^c Pont et al. 2004, ^d Bouchy et al. 2004, ^e Alonso et al. 2004

$$\cos i = \frac{R_*}{a} \left\{ \frac{(1 - \sqrt{\Delta F})^2 - [\sin^2(t_F \pi / P) / \sin^2(t_T \pi / P)](1 + \sqrt{\Delta F})^2}{1 - [\sin^2(t_F \pi / P) / \sin^2(t_T \pi / P)]} \right\}^{\frac{1}{2}}, \quad (5)$$

where G is the gravitational constant, and t_T and t_F denote the total transit duration and the “flat-bottom” duration, respectively.

We attempted to compute the orbital elements of OGLE and TrEs planets using the above equations. The result is shown in Table 2. We found that while the estimated periods are different from the actual ones by several hours, the semi-major axes and the inclinations agree within around 0.01 AU and a few degrees, respectively.

In order to derive the transit depth, the transit duration and the flat-bottom duration, we need a template light curve for the fit. For that purpose, we use the perturbation result derived by Ohta, Taruya, & Suto (2005). The template flux is given as

$$F = 1 - \frac{f(\gamma, \rho)}{\pi(1 - u_1/3 - u_2/6)}. \quad (6)$$

Here, u_1 , u_2 are limb darkening parameters and they are defined as

$$I(\mu)/I(0) = [1 - u_1(1 - \mu) - u_2(1 - \mu)^2]. \quad (7)$$

Here, μ is an angle between the star’s radius vector and the line of sight. Moreover, $f(\gamma, \rho)$ is given as

$$f(\gamma, \rho) = \begin{cases} \pi\gamma^2 [1 - u_1 - u_2(2 - \rho^2 - \frac{1}{2}\gamma^2) + (u_1 + 2u_2)W_1] & \rho < 1 - \gamma \\ (1 - u_1 - \frac{3}{2}u_2) \left[\gamma^2 \cos^{-1} \left(\frac{\zeta}{\gamma} \right) + \sin^{-1} z_0 - \rho z_0 \right] \\ + \frac{1}{2}u_2\rho \left[(\rho + 2\zeta)\gamma^2 \cos^{-1} \left(\frac{\zeta}{\gamma} \right) - z_0(\rho\zeta + 2\gamma^2) \right] \\ + (u_1 + 2u_2)W_3 & 1 - \gamma < \rho < 1 + \gamma \\ 0 & \rho > 1 + \gamma, \end{cases} \quad (8)$$

where γ , ρ , η_p , z_0 , ζ are defined as

$$\gamma = R_p/R_*, \quad (9)$$

$$\rho = 1 + \eta_p = \frac{\sqrt{X_p^2 + Z_p^2}}{R_*} \quad (10)$$

$$z_0 = \frac{\sqrt{(\gamma^2 - \eta_p^2)[(\eta_p + 2)^2 - \gamma^2]}}{2(1 + \eta_p)} \quad (11)$$

$$\zeta = \frac{2\eta_p + \gamma^2 + \eta_p^2}{2(1 + \eta_p)}. \quad (12)$$

Here, X_p and Z_p are the positions of the center of the planet in the star’s central coordinate system. W_1 and W_3 are integrals which are defined in the Appendix of Ohta, Taruya, & Suto (2005). For simplicity, we do not consider the effect of limb darkening ($u_1 = u_2 = 0$). After the fit, we obtain the orbital elements by substituting the values of ΔF , t_F , and t_T into equations (1) and (3) to (5).

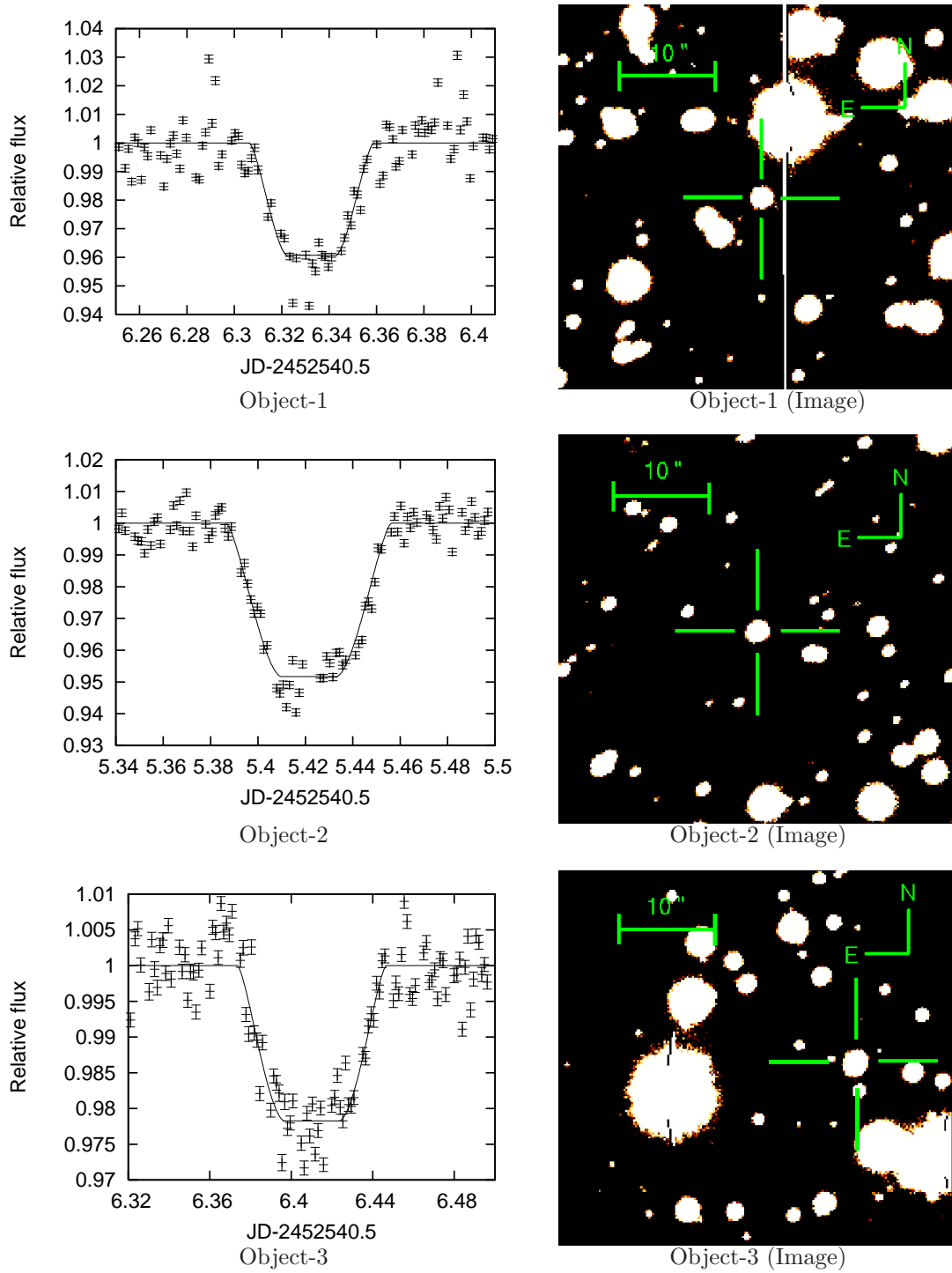


Fig. 4. *Left:* Light curves for the single transiting candidates. The best-fit light curve models are based on Ohta, Taruya, & Suto (2005). We assume a K0 dwarf for Object-1 and Object-3, and a K5 dwarf for Object-2. *Right:* Images for the single transiting candidates. Object-3 turns out to be a double star.

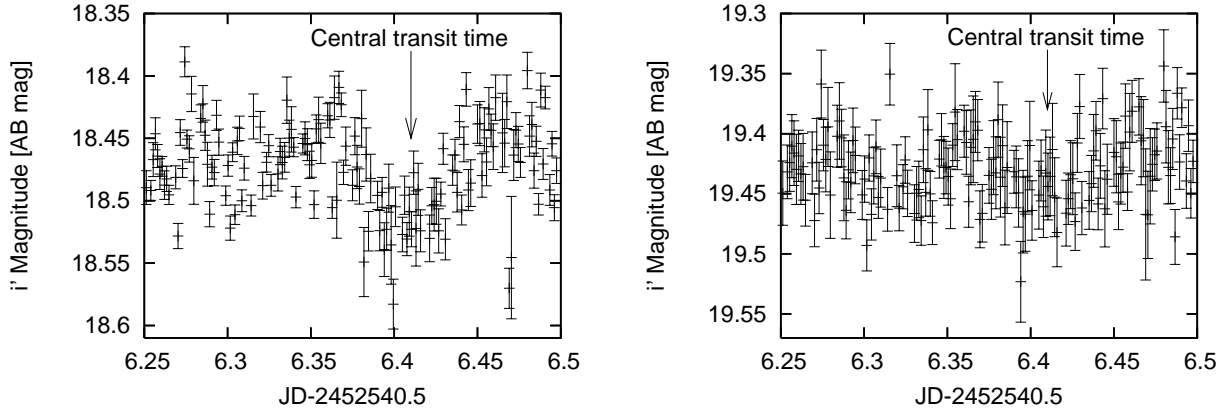


Fig. 5. Light curves of Object-3-A (*Left*) and Object-3-B (*Right*) from the PSF photometry. The arrows indicates the central transit time estimated from Figure 4.

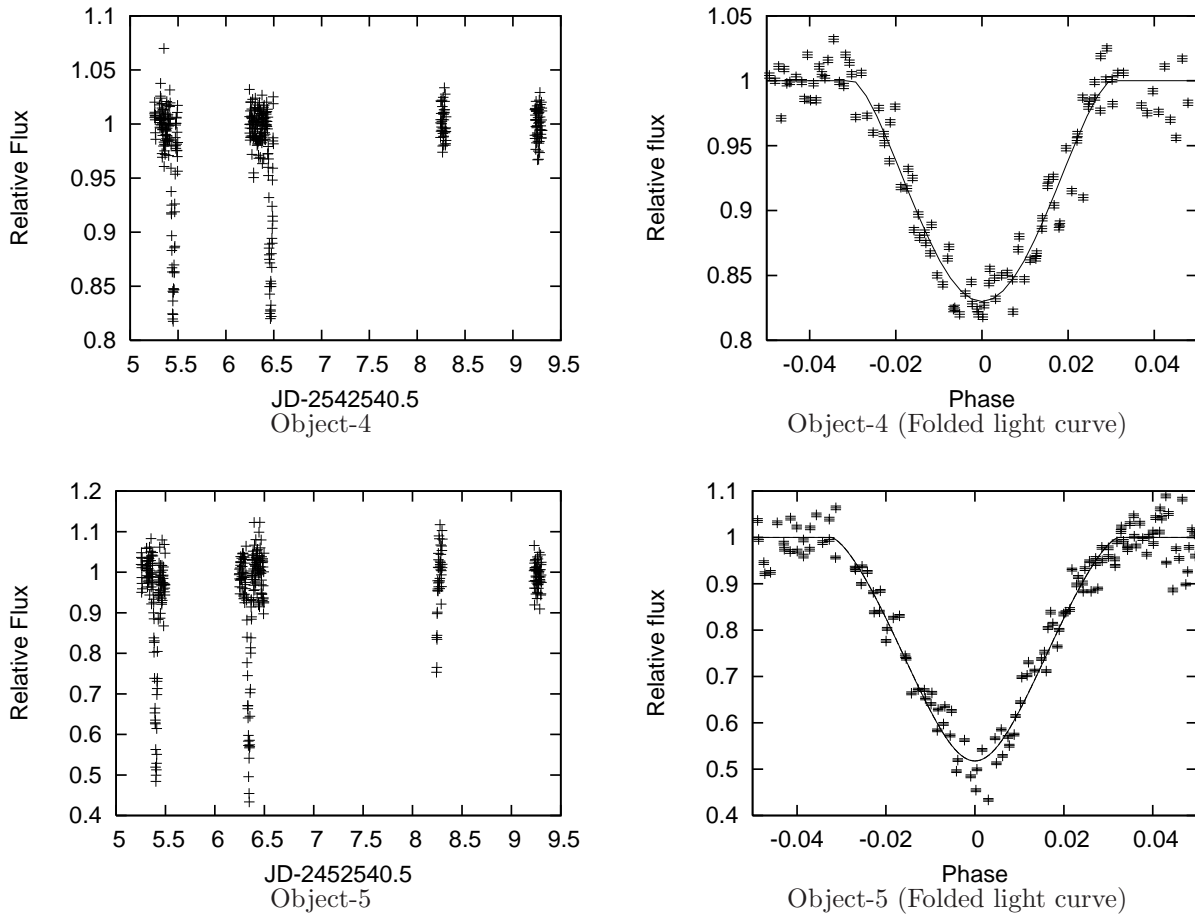


Fig. 6. *Left:* Light curves for the double transiting candidates during this observing run. *Right:* Folded light curves. The best-fit light curve models are based on Ohta, Taruya, & Suto (2005). We assume a K5 dwarf for Object-4. For Object-5 whose spectral type is unknown, we tentatively assume $1 R_{\odot}$ for its parent star.

Table 3. Observed parameters for the transiting candidates.

Object	RA	Dec	B [mag]	R _c [mag]	i' [AB mag]	z' [AB mag]
Object-1	21 ^h 13 ^m 35 ^s .7	48°15'20''6	21.55±0.02	18.84±0.04	18.34±0.05	17.69±0.04
Object-2	21 ^h 13 ^m 37 ^s .2	48°10'37''8	22.04±0.02	19.04±0.03	18.50±0.05	18.01±0.04
Object-3-A	21 ^h 11 ^m 42 ^s .5	48°9'46''4	21.13±0.02	18.74±0.02	18.47±0.03	18.04±0.03
Object-3-B	21 ^h 11 ^m 42 ^s .5	48°9'47''0	23.32±0.09	20.10±0.03	19.40±0.03	18.71±0.03
Object-4	21 ^h 13 ^m 17 ^s .7	48°6'43''7	23.73±0.06	20.63±0.03	19.86±0.05	19.28±0.04
Object-5	21 ^h 13 ^m 12 ^s .0	48°18'0''6	—	21.89±0.07	20.53±0.05	19.81±0.06

Table 4. Estimated parameters for the transiting candidates assuming they are dwarfs. Total transit duration and the flat-bottom duration are represented by t_T and t_F , respectively.

Object	SpT	A _V [mag]	ΔF [%]	t_T [min]	t_F [min]	P [day]	a [AU]	i [°]	Dist [kpc]	Radi [R _{Jup}]
Object-1	G0V/K5V	3.1	3.9±0.8	76-92	0-34	0.3-1.8	0.01-0.02	67-84	1.0-3.0	1.4-2.2
	M0V/M5V	1.1	4.4±0.8	91-111	0	2.1-6.9	0.02-0.03	86-89	0.3-1.2	0.6-1.3
Object-2	K5V/M0V	1.1	4.9±0.5	101-106	23-34	1.5-2.5	0.02-0.03	84-86	1.3-2.3	1.3-1.6
Object-3-A	K0V/M2V	1.4	3.2±0.7	106-111	0-39	1.7-5.6	0.03-0.05	83-88	1.2-3.0	0.9-1.5
Object-4	K5V/M0V	1.6	17.0±1.6	86-93	0	1.018	0.02	84	2.3-4.0	2.5-3.0
Object-5	—	—	48.2±4.2	90	0	0.942	—	—	—	—

4. Candidate Transiting Objects

After visual inspection of around 1000 objects which satisfied our selection criteria, we found five strong transit candidates; three objects (Object-1, Object-2 and Object-3-A) exhibit a single full transit-like event. Their fractional flux decrements ($\sim 5\%$) for a couple of hours are consistent with a planetary transit, and spectroscopic photometric and/or photometric follow-up observations is justified. The other two objects (Object-4 and Object-5) show double transit events, and their transit depths indicate that they are binary star systems. Further information of those candidates is summarized in Tables 3 and 4, and their lightcurves are shown in Figure 4 to Figure 6. The error in the transit depth quoted in Table 4 corresponds to the standard deviation of the baseline flux of the light curve during the out-of-transit phase. We briefly discuss each object below.

4.1. Object 1

Multicolor photometry indicates that Object-1 ($i'=18.34$ AB mag) is either a G0/K5 or an M0/M5 star. It is likely that Object-1 is a dwarf because its distance exceeds the Galaxy scale (> 17 kpc) if it is a giant. Adopting typical parameters for a G0/K5 or M0/M5 dwarf, we estimate the companion size and orbital elements using equations (1) and (3) to (5) which are summarized in Table 4.

Depending on the choice of the spectral type, and therefore the adopted radius, of the parent star, the companion takes two different sets of parameters. If it is an M dwarf and A_V is derived from its observed color and an unreddened standard M2 dwarf, the distance is estimated as 0.3-1.2 kpc. The companion radius is $(0.6 - 1.3)R_J$, the orbital period is 2.1-6.9 day, the semi-major axis is 0.02-0.03 AU, and the inclination is 86-89°. This set of parameter is consistent with a Jupiter size companion.

4.2. Object 2

Multicolor photometry indicates that Object-2 ($i'=18.50$ AB mag) is likely to be a late K giant, but if it is a giant, the inferred distance of 84 kpc exceeds the Galaxy's size. Moreover, given the observed scatter of objects in Figure 2, a dwarf could well be located at the position of Object-2 in the color-color diagram. Therefore, it is quite possible that Object-2 is a K5/M0 dwarf. Adopting this interpretation, we obtain a distance of 1.3-2.3 kpc, a companion radius of $(1.3 - 1.6)R_J$, an orbital period of 1.5-2.5 days, a semi-major axis of 0.02-0.03 AU, and an inclination of 84-86°.

4.3. Object 3

Object-3 turned out to be a very close double star with a separation of ~ 0.6 arcsec; their individual fluxes cannot be separated via aperture photometry. So we reanalyzed Object-3 using PSF photometry. The results are shown in Figure 5. We find that Object-3 consists of Object-3-A ($i' = 18.47$ AB mag) and Object-3-B ($i' = 19.40$ AB mag) and the transit-like feature preferentially appears in Object-3-A.

Multicolor photometry suggests that Object-3-A is a K0/M2 star. We estimate the depth, the transit durations and the flat-bottom durations from the model light curves plotted in Figure 4 since the lightcurve for Object-3-A from

the PSF photometry is noisier and still may not completely free from flux contamination of Object-3-B. Ascribing the total flux decrement to a companion around Object-3-A, we derive the transit depth of Object-3-A is 3.2% using the mean brightness ratio of Object-3-A and Object-3-B from the PSF photometry.

Assuming that a companion orbits around a K0/M2 dwarf, the distance is 1.3-2.3 kpc and the companion radius is $(0.9 - 1.5)R_J$, the orbital period is 1.7-5.6 days, the semi-major axis is 0.03-0.05 AU, and the inclination is 83-88°.

4.4. Object 4

Object-4 ($i' = 19.86$ AB mag) exhibited double transits of a fairly large depth of $17.0 \pm 1.6\%$. The PDM method suggests an orbital period of 1.018 days, and multicolor photometry indicates that Object-4 is a K5/M0 star. The light curve has a transit duration of 86-93 minutes and does not show a flat-bottomed shape. Assuming that Object-4 is a K5/M0 dwarf, the distance is 2.3-4.0 kpc. For a circular-orbiting companion, the semi-major axis is 0.02 AU, the inclination is 84°, the companion radius is $(2.5 - 3.0)R_J$. Thus the companion of Object-4 is likely to be a late M dwarf. Since the observing run did not cover the full phase, we were unable to detect a secondary eclipse.

4.5. Object 5

Object-5 ($i' = 20.53$ AB mag) also exhibited double transits of a significant depth of $48.2 \pm 4.2\%$. Because of the large depth, Object-5 is likely to be an eclipsing binary system with an orbital period of 0.942 days. Because Object-5 is very faint, we were not able to identify Object-5 in our *B*-band data. Thus we cannot determine its spectral type and the other parameters.

5. Summary and Discussion

We have carried out a photometric search for transiting extrasolar planets using Subaru Suprime-Cam. Out of about 100,000 stars monitored, we obtain 7,700 (27,000) light curves with photometric precision below 1% (3%), required to detect extrasolar planets by the transit method. This result thus demonstrates that Suprime-Cam indeed has the photometric stability and accuracy required for a transiting planet survey.

During this observing run, we detected three transiting planetary candidates (*i'*-band magnitude around 18.5) which exhibit a single full transit-like light curve with a depth of $< 5\%$. Thus it is worthwhile attempting spectroscopic and photometric follow-up observations of these candidates. Adopting typical parameters for the parent stars from their spectral type, we infer that their semi-major axes are less than 0.05 AU. If a Jupiter mass object orbits at a distance of 0.05 AU from a central star of $1 M_\odot$ star, the radial velocity amplitude exceeds 100 m/s. A faint ($i' \sim 18.5$) object with 100 m/s radial velocity would be detectable via a normal Tr-Ar wavelength calibration (i.e., without an iodine cell) with 7,200 second exposures per frame using the high-dispersion spectrograph of a large telescope, such as Subaru, HDS (Noguchi et al. 2002; Sato et al. 2002; Winn et al. 2004; Narita et al. 2005).

Finally we discuss a strategy of follow-up photometry and possible future transit surveys using Subaru. The predicted detection number N_p of very hot Jupiters by a transit survey is roughly estimated as follows

$$N_p \sim N F_p P_{vis}. \quad (13)$$

Here, N is the observed number of single FGKM dwarfs that have an adequate photometric precision for very hot Jupiters detections, F_p is the fraction of field stars that accompany transiting very hot Jupiters, and P_{vis} is the probability that at least double full transits will occur during the observing run (Mallén-Ornelas et al. 2003). In our observations, a photometric precision within 3.0% is achieved for approximately 27,000 objects. Assuming that most of them are dwarf and the binary fraction is 0.5, the expected value of N is 13,500. F_p is one in 3300-6700 single main sequence FGK stars for very hot Jupiters according to Gaudi, Seager, & Mallén-Ornelas (2005). If we conduct continuous 9 hours of observation each night for 10 days, P_{vis} is 0.49 and N_p is approximately 1.0-2.0. A longer observing run is needed to increase P_{vis} for detection of multiple transits. Given the highly competitive time allocation for Subaru, it is not realistic to look for the multiple transit features of (very) hot Jupiters. Our current result showed, however, that single transit candidates can be located with Suprime-Cam relatively easily. Moreover, a future transit survey of a denser region of stars due to the good seeing at Subaru site would make it possible to detect more single transit candidates. Then those candidates could be observed for follow-up photometry with a smaller telescope. For instance, we plan to attempt follow-up of our candidates ($i' \sim 18.5$) with the Nayuta (2 m telescope of Nishiharima Astronomical Observatory, Japan) and the 1.5 m telescope of Gunma Astronomical Observatory. Since the transit depth of our candidates is approximately 4%, we would be able to detect multiple transit features with 120-360 second exposures using these telescopes. Such complementary observations by a 2 m class telescope would make the transit survey using a very large telescope more effective and productive and lead to confirmed detection of extrasolar planets.

We thank Yasuhiro Ohta for providing us with a numerical routine to compute the lightcurve of planetary transits. This work is supported by a Grant-in-Aid for JSPS Fellows (No.52791) and “The 21st Century COE Program of

Table 5. Observed parameters for W UMa-like objects.

Object	RA	Dec	B [mag] (Phase)	R _c [mag] (Phase)	i' [AB mag] (Phase)	z' [AB mag] (Phase)
Object-6	21 ^h 13 ^m 24 ^s .1	48°29'49"9	23.20±0.05 (0.61)	19.66±0.03 (0.79)	18.78±0.10 (0.78)	18.04±0.04 (0.82)
Object-7	21 ^h 12 ^m 29 ^s .2	48°7'31"8	21.83±0.03 (0.56)	19.28±0.03 (0.94)	19.08±0.06 (0.43)	18.65±0.05 (0.98)
Object-8	21 ^h 11 ^m 4 ^s .9	48°8'3"6	22.54±0.04 (0.35)	19.53±0.03 (0.22)	18.95±0.06 (0.61)	18.18±0.05 (0.26)
Object-9	21 ^h 12 ^m 1 ^s .0	48°17'29"2	24.33±0.13 (0.69)	21.45±0.04 (0.48)	20.48±0.03 (0.17)	19.83±0.03 (0.52)
Object-10	21 ^h 10 ^m 33 ^s .1	48°15'20"7	24.40±0.09 (0.76)	20.86±0.03 (0.61)	20.38±0.06 (0.64)	19.39±0.05 (0.88)
Object-11	21 ^h 10 ^m 31 ^s .9	48°8'18"5	23.91±0.07 (0.95)	20.83±0.04 (0.70)	20.21±0.06 (0.73)	19.39±0.05 (0.34)
Object-12	21 ^h 10 ^m 27 ^s .8	48°14'30"8	24.34±0.10 (0.75)	20.81±0.03 (0.47)	20.39±0.06 (0.50)	19.35±0.06 (0.20)
Object-13	21 ^h 11 ^m 23 ^s .9	48°11'43"7	22.10±0.05 (0.06)	19.34±0.03 (0.66)	19.28±0.06 (0.09)	18.53±0.06 (0.69)
Object-14	21 ^h 11 ^m 37 ^s .4	48°21'45"5	22.95±0.05 (0.75)	19.93±0.03 (0.47)	19.40±0.05 (0.50)	18.64±0.03 (0.20)
Object-15	21 ^h 10 ^m 50 ^s .9	48°32'18.5	21.39±0.03 (0.34)	18.54±0.03 (0.02)	18.19±0.05 (0.93)	17.55±0.03 (0.04)
Object-16	21 ^h 10 ^m 21 ^s .1	48°22'20"1	21.48±0.04 (0.70)	19.04±0.03 (0.61)	18.73±0.05 (0.85)	18.21±0.04 (0.65)

Origin and Evolution of Planetary System” from the Ministry of Education, Culture, Sports, and Technology.

Appendix 1. W UMa-like eclipsing binary candidates

We also detected eleven W UMa-like objects whose period is less than 0.4 days. The light curves are shown in Figure 7. The observational results are shown in Table 5 and Table 6. In order to determine the distance, we used the color-magnitude relation and period-color relation (Rucinski 1998) for the spectral type between early F and middle K stars. These are written as

$$M_V = -4.44 \log P + 3.02(B - V) + 0.12, \quad (\text{A1})$$

$$(B - V) = 0.04 \times P^{-2.25}. \quad (\text{A2})$$

Here M_V is the absolute magnitude and P is the period. Substituting equation (A2) for equation (A1), we can calculate the absolute magnitude without observations for the B band and V band. If the spectral type of objects is not between early F and middle K, the distance is estimated by the typical absolute magnitude for the spectral type of the objects.

Object-6: The amplitude is approximately 2%. The period is 0.309 days. Multicolor photometry suggests a K5/M2 star. If Object-6 is a dwarf, the distance is 0.7-1.7 kpc.

Object-7: The primary minimum and the secondary minimum are approximately 5% and 3%, respectively. The period is 0.225 days. Multicolor photometry suggests a K0/ M2 star. The distance of 3.1 kpc obtained from equation (A1) and equation (A2).

Object-8: The amplitude is approximately 3%. The period is 0.254 days. Multicolor photometry suggests a F8/K2 or M2/M5 star. If Object-8 is a F8/K2 dwarf, the distance is 1.6 kpc. In the case of an M2/M5 dwarf, the estimated distance of 0.4-1.1 kpc is obtained from its expected absolute magnitude.

Object-9: The primary and secondary minimums are approximately 12% and 7%, respectively. The period is 0.260 days. Multicolor photometry suggests a G5/K5 or an M2/M5 star. If Object-9 is a G5/K5 dwarf, the distance is 6.7 kpc. In the case of an M2/M5 dwarf, the estimated distance is 1.3-3.3 kpc.

Object-10: The amplitude is approximately 10%. The period is 0.346 days. Multicolor photometry suggests a F5/K2 or an M2/M5 star. If Object-10 is a F5/K2 dwarf, the distance is 5.4 kpc. In the case of an M2/M5 dwarf, the estimated distance is 0.5-1.3 kpc.

Object-11: The amplitude is approximately 10%. The period is 0.358 days. Multicolor photometry suggests a F8/K2 or M2/M5 star. If Object-11 is a F8/K2 dwarf, the distance is 9.3 kpc. In the case of an M2/M5 dwarf, the

Table 6. Estimated parameters for W UMa-like objects assuming they are dwarfs.

Object	Spectral type	Period [days]	Amplitude		Distance [kpc]
			Primary	Secondary[%]	
Object-6	K5V/M2V	0.309	2		0.7-1.7
Object-7	K0V/M2V	0.225	5 3		3.1
Object-8	F8V/K2V or M2V/M5V	0.254	3		1.6 or 0.4-1.1
Object-9	G5V/K5V or M2V/M5V	0.260	12 7		6.7 or 1.3-3.3
Object-10	F5V/K2V or M2V/M5V	0.346	10		5.4 or 0.5-1.3
Object-11	F8V/K2V or M2V/M5V	0.358	10		9.3 or 0.7-1.9
Object-12	F0V/G8V	0.362	18 15		5.1
Object-13	F0V/K0V	0.270	15 13		2.1
Object-14	G5V/K5V or M0V/M5V	0.259	3		2.8 or 0.4-1.6
Object-15	G0V/K7V or M0V/M5V	0.368	8 6		5.8 or 0.3-1.2
Object-16	G5V/K5V or M0V/M5V	0.252	2		2.5 or 0.5-1.9

estimated distance is 0.7-1.9 kpc.

Object-12: The primary and secondary minimums are approximately 18% and 15%, respectively. The period is 0.362 days. Multicolor photometry suggests a F0/G8 star. If Object-12 is a dwarf, the distance is 5.1 kpc.

Object-13: The primary and secondary minimums are approximately 15% and 13%, respectively. The period is 0.270 days. Multicolor photometry suggests a F0/K0 star. If Object-13 is a dwarf, the distance is 2.1 kpc.

Object-14: The amplitude is approximately 3%. The period is 0.259 days. Multicolor photometry suggests a G5/K5 or an M0/M5 star. If Object-14 is a G5/K5 dwarf, the distance is 2.8 kpc. In the case of an M0/M5 dwarf, the estimated distance is 0.4-1.6 kpc.

Object-15: The primary and secondary minimums are approximately 8% and 6%, respectively. The period is 0.368 days. Multicolor photometry suggests a G0/M5 star. If Object-15 is a G0/K7 dwarf, the distance is 5.8 kpc. In the case of an M0/M5 dwarf, the estimated distance is 0.3-1.2 kpc.

Object-16: The amplitude is approximately 2%. The period is 0.252 days. Multicolor photometry suggests a G5/K5 star or an M0/M5 star. If Object-16 is a G5/K5 dwarf, the distance is 2.5 kpc. In the case of an M0/M5 dwarf, the estimated distance is 0.5-1.9 kpc.

References

- Abe, F., et al. 2005, MNRAS, 364, 325
Alonso, R., et al. 2004, ApJ, 613, L153
Basri, G., Borucki, W.J., & Koch, D. 2005, NewAR, 49, 478
Bessell, M. S. 1990 PASP, 102, 1181
Bouchy, F., Pont, F., Santos, N.C., Melo, C., Mayor, M., Queloz, D., & Udry, S. 2004, A&A, 421, L13
Bordé, P., Rouan, D., & Léger, A., 2003, A&A, 405, 1137
Borucki, W.J., Caldwell, D., Koch, D.G., Webster, L.D., Jenkins, J.M., Ninkov, Z., & Showen, R. 2001, PASP, 113, 439
Christian, D.J., et al. 2004, in ESO Conf. Proc., Cool Stars 13, in press
Cox, A.N., 2001, Allen's Astrophysical Quantities (New York, AIP) 389
Fukugita, M., Ichikawa, T., Gunn, J. E., Doi, M., Shimasaku, K., & Schneider, D. P. 1996, AJ, 111, 1748
Gaudi, B.S., Seager, S., & Mallén-Ornelas, G. 2005, ApJ, 623, 472
Hood, B., et al. 2005, MNRAS, 360, 791
Konacki, M., Torres, G., Sasselov, D. D., & Jha, S. 2003a, Nature, 421, 507
Konacki, M., Torres, G., Sasselov, D. D., & Jha, S. 2003b, ApJ, 597, 1076
Konacki, M., Torres, G., Sasselov, D. D., & Jha, S. 2005, ApJ, 624, 372
Lomb, N.R. 1976, Ap&SS, 39, 447
Mallén-Ornelas, G., Seager, S., Yee, H.K.C., Minniti, D., Gladders, M.D., Mallén-Fullerton, G.M., & Brown, T.M. 2003, ApJ, 582, 1123
Mayor, M., & Queloz, D. 1995, Nature, 378, 355
Miyazaki, S., et al. 2002 PASJ, 54, 833
Narita, N., Suto, Y., Winn, J. N., Turner, E. L., Aoki, W., Leigh, C.J., Sato, B., Tamura, M., & Yamada, T. 2005, PASJ, 57, 471
Noguchi, K., et al. 2002, PASJ, 54, 855
Ohta, Y., Taruya, A., & Suto, Y. 2005 ApJ, 622, 1118
Oke, J. B. 1990 AJ, 99, 1621
Ouchi, M., et al. 2004, ApJ, 611, 660
Pont, F., Bouchy, F., Queloz, D., Santos, N.C., Melo, C., Mayor, M., & Udry, S. 2004, A&A, 426, L15
Press, W. H., Teukolsky, A. T., Vetterling, W. T., Flannery, B. P. 1992, "Numerical Recipes in FORTRAN" (New York, Cambridge University Press), 569
Rucinski, S. M. 1998, AJ, 116, 2998
Sato, B., Kambe, E., Takeda, Y., Izumiura, H., & Ando, H. 2002, PASJ, 54, 873
Seager, A., & Mallén-Ornelas, G. 2003, ApJ, 585, 1038
Stellingwerf, R. F. 1978, ApJ, 224, 953
Torres, G., Konacki, M., Sasselov, D. D., & Jha, S. 2004, ApJ, 609, 1071
Udalski, A., et al. 2002, AcA, 52, 1
Udalski, A., Szewczyk, O., Zebun, K., Pietrzynski, Z., Szymandki, M., Kubiak, M., Soszynski, I., & Wyrzykowski, L. 2002, AcA, 52, 317
Weldrake, D.T.F., & Sackett, P.D. 2005, ApJ, 620, 1043
Winn, J. N., Suto, Y., Turner, E. L., Narita, N., Frye, B. L., Aoki, W., Sato, B., & Yamada, T. 2004, PASJ, 56, 655

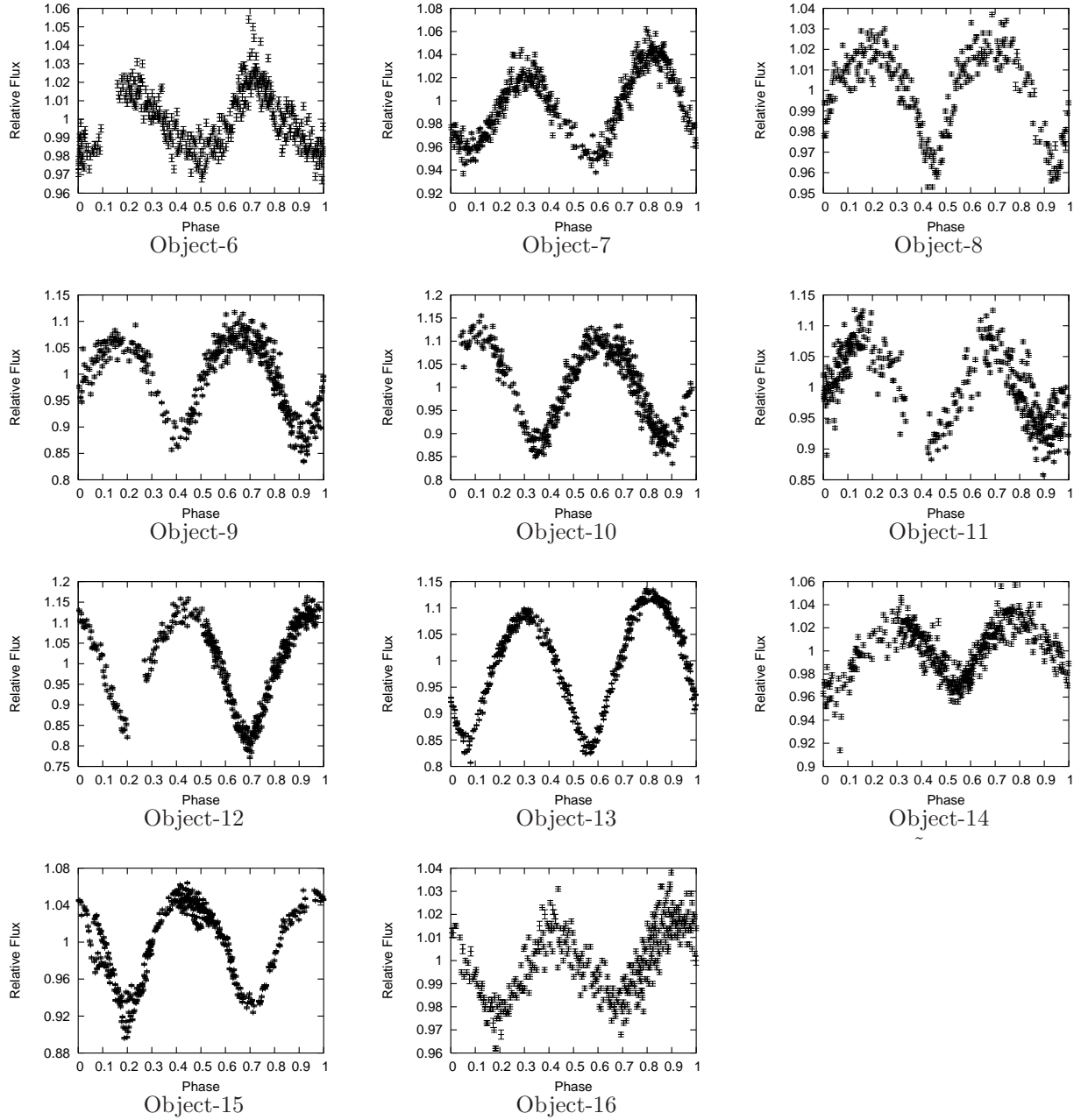


Fig. 7. Light curves of W UMa objects.

Yagi, M., Kashikawa, N., Sekiguchi, M., Doi, M., Yasuda, N., Shimasaku, K., & Okamura, S. 2002, AJ, 123, 66

